Simultaneous measurement of RBC velocity, flux, hematocrit and shear rate in vascular networks

Walid S Kamoun[1], Sung-Suk Chae[1], Delphine A Lacorre[1], James A Tyrrell[2], Mariela Mitre[1], Marijn A Gillissen[1], Dai Fukumura[1], Rakesh K Jain[1] & Lance L Munn[1]

Not all tumor vessels are equal. Tumor-associated vasculature includes immature vessels, regressing vessels, transport vessels undergoing arteriogenesis and peritumor vessels influenced by tumor growth factors. Current techniques for analyzing tumor blood flow do not discriminate between vessel subtypes and only measure average changes from a population of dissimilar vessels. We developed methodologies for simultaneously quantifying blood flow (velocity, flux, hematocrit and shear rate) in extended networks at single-capillary resolution *in vivo*. Our approach relies on deconvolution of signals produced by labeled red blood cells as they move relative to the scanning laser of a confocal or multiphoton microscope and provides fully resolved three-dimensional flow profiles within vessel networks. Using this methodology, we show that blood velocity profiles are asymmetric near intussusceptive tissue structures in tumors in mice. Furthermore, we show that subpopulations of vessels, classified by functional parameters, exist in and around a tumor and in normal brain tissue.

Tumor blood vessels are heterogeneous in their structure and function, probably owing to differential exposure to growth factors in the microenvironment and nonsynchronous progression of angiogenesis and maturation[1–4]. Because of technical limitations, most measurements of tumor vessel function are performed on single vessels or are measured as bulk parameters over a large network. This limits our ability to detect responses to vessel-targeted drugs, which usually affect specific subpopulations of vessels. To determine how individual vessels, or classes of vessels, are involved in tumor growth and response to treatment, tools for studying blood flow in extended vessel networks, at the spatial resolution of single capillaries, are urgently needed.

Many techniques have been used to analyze tumor hemodynamics. Single-photon video-rate imaging has for many years been the standard method for measuring blood flow in normal and tumor vessels[1–3]. Coupled with algorithms for automated detection and tracking of fluorescently labeled red blood cells (RBCs)[5] or two-slit and four-slit cross-correlation methods[6], this allows flow analysis in single vessels. However, single-photon techniques have relatively poor spatial resolution in the z direction (along the light path) and are less accurate when the vessels do not lie in the x–y plane.

Recently, a multiphoton laser scanning microscopy (MPLSM)-based technique for single-vessel blood-flow analysis using line scanning has been developed to quantify blood flow in individual cerebral cortical capillaries[7] and tumor blood vessels[8]. This axial line scanning (ALS) quantifies flow velocity in selected blood vessels by scanning along the central axis of the blood vessel at high frequency, relying on contrast between an injected plasma fluorophore and the erythrocytes, which are dark. In an intensity plot of location along the line scan against time, streaks are produced with angles that are proportional to the velocity of RBCs (**Fig. 1a**). Line scanning along the central axis of a vessel allows centerline velocity to be quantified, and this can be used to estimate average flow velocity. ALS has good accuracy and sensitivity, especially when implemented with appropriate analysis algorithms[9]. It can be used to measure a wide range of velocities but does not allow accurate quantification of erythrocyte flux (number of RBCs per second) or hematocrit (fraction of blood volume occupied by RBCs). Also, as there are generally more vessels than can be analyzed in a single session, this approach is subjective, as the operator must choose which vessels to measure.

To overcome these limitations, we developed two MPLSM-based methods for blood-flow analysis in tumor and normal vascular networks. The first method, residence time line scanning (RTLS), allows direct analysis of flow velocity by scanning a line at an arbitrary angle to the vessel (**Fig. 1a**). The second method, relative velocity field scanning (RVFS), is a full-field method that allows simultaneous analysis of most of the vessels in a field of view by deconvolving the image distortion produced by the moving cells relative to the moving laser scans (**Fig. 1b**). Here we describe the operational principles of RTLS and RVFS, and demonstrate the power of the methodologies, first by measuring fully resolved lumenal profiles of velocity, flux, hematocrit and shear rate in tumor vessels undergoing intussusceptive angiogenesis, and second by performing cluster analyses to identify 'signatures' of vessels based on location and function.

[1]Edwin L. Steele Laboratory, Department of Radiation Oncology, Massachusetts General Hospital and Harvard Medical School, Boston, Massachusetts, USA. [2]Thomson Reuters, Corporate Research & Development, New York, New York, USA. Correspondence should be addressed to L.L.M. (munn@steele.mgh.harvard.edu).

RECEIVED 1 FEBRUARY; ACCEPTED 24 MAY; PUBLISHED ONLINE 27 JUNE 2010; DOI:10.1038/NMETH.1475

RESULTS

RTLS operational principles

To perform either RTLS or RVFS, we labeled RBCs *ex vivo* with a far-red lipophilic fluorescent dye (1,1-dioctadecyl-3,3,3,3-tetramethylindodicarbocyanine perchlorate (DID)) that allowed us to use MPLSM to observe deep in the tissue. We mixed the labeled RBCs with the endogenous mouse blood by systemic injection at a ratio of 3–5 labeled RBCs per 100 RBCs; the labeled RBCs are ideal for long-term studies, with a half-life of approximately 10–14 d in the circulation, comparable to erythrocyte half-life in mice[10]. We performed RTLS by scanning along a single line that intersects the vessel (**Fig. 1a** and **Supplementary Fig. 1a**). Repeated scanning along this line generated fluorescence intensity data along the line over time (x–t), in which 'images' of the fluorescent RBCs are compressed or elongated depending on the residence time of the cells in the scan. The length of each cell signal in the x–t domain along the time axis depends on the number of times the laser scans the fluorescent cell as it passes. Thus, we can extract velocities from the line scan frequency, scanning angle and the length of the x–t cell images.

As RBCs are biconcave flat discs (~1 μm thick, 7 μm in diameter) that tumble in the bloodstream, they can have various orientations when crossing the scan line; this could affect their x–t cell image independently of their velocity. To rigorously and directly test the potential error owing to orientation, we directly compared RTLS with ALS, a method that is insensitive to RBC

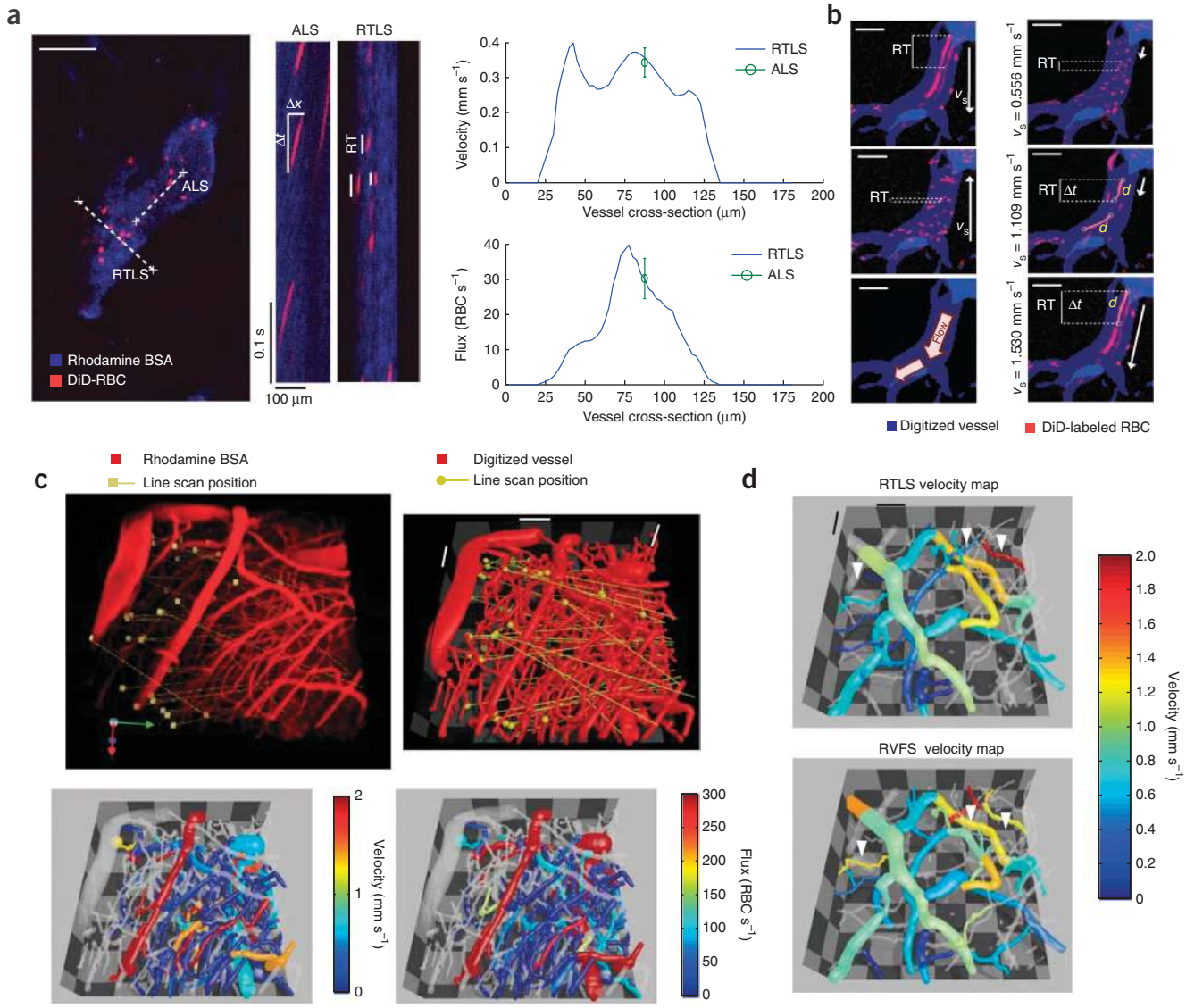

Figure 1 | Description, validation and application of RTLS and RVFS. (**a**) Representative MPLSM angiogram of a tumor blood vessel (left). We generated x versus t plots by scanning along the centerline of the vessel with ALS and perpendicular to the vessel with rtls. Analysis of flow velocity is based on the slope of the RBC signal ($\Delta x/\Delta t$) for ALS and on residence time (RT) for RTLS. RBC velocity and flux measured along the vessel cross-section using RTLS were compared to ALS-based analysis of flow (right; mean ± s.e.m.). (**b**) Multiphoton images of a single vessel scanned with of the indicated scanning velocities (v_s) in two opposing scanning directions. Scanning from top to bottom with velocities from 1.1 to 1.5 mm s^{-1} caused 'velocity-matched' RBCs with higher RT values and a measurable traveled distance (d). (**c**) Three-dimensional MPLSM angiogram of the brain of a tumor-bearing mouse illustrating the position of the line scans at several z planes (top on the left is the multiphoton image volume, and on the right is the segmented network resulting from the segmentation algorithm). Comprehensive velocity and flux 3D maps generated using RTLS (bottom). (**d**) Three-dimensional velocity map of a glioma network analyzed by RTLS and RVFS. Vessels in which RVFS velocity measurement differed from RTLS owing to low RBC flux are indicated by arrowheads. Scale bars, 100 μm (**a**,**c**,**d**) and 50 μm (**b**).

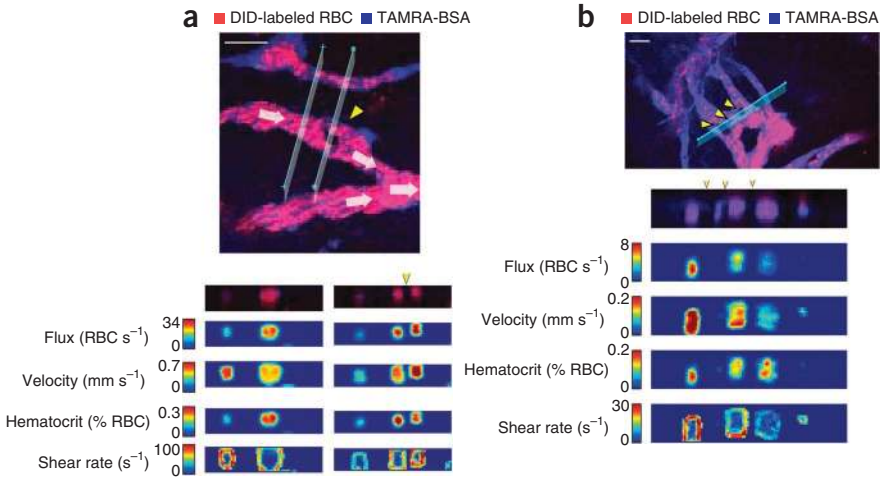

Figure 2 | Analysis of cross-sectional flow profiles in tumor vessels undergoing intussusceptive angiogenesis. (**a**,**b**) Multiphoton images with planes indicating where the cross-sectional line scanning was done. Cross-sectional velocity, flux, hematocrit shear rate profiles and raw data maps upstream and at the level of single (**a**) or multiple (**b**) intussusceptions (arrowheads). Arrows in **a** indicate direction of flow. Scale bars, 50 μm.

orientation (**Supplementary Fig. 2**). We found good correspondence between the two techniques, with no apparent biases at the low or high velocity ranges.

An important advantage of RTLS is that, compared with ALS, it is relatively insensitive to the orientation of the scan line with respect to the vessel. This means that RTLS scans can be randomly placed or systematically arranged (for example, in a grid pattern), removing operator dependence. Furthermore, each scan can intersect several vessels, allowing simultaneous measurement of multiple velocity profiles (**Fig. 1c** and **Supplementary Fig. 1a**). The technique is sufficiently robust to map velocities and fluxes in complex glioma vasculatures with its abundance of small vessels (**Fig. 1c**).

Although RTLS has advantages over ALS, it has certain limitations. Blood velocity can vary markedly along a given tumor vessel owing to abrupt changes in diameter or the presence of bifurcations, and RTLS still only analyzes a subset of these vessel cross-sections. Another approach, therefore, might be to perform full-field imaging at sufficiently high frame rates and use cell-tracking algorithms or correlation analyses to calculate blood flow throughout a network. Unfortunately, full-field acquisition rates for standard confocal and multiphoton microscopes are too slow to be used in this way.

RVFS operational principles

To circumvent the slow acquisition rates, of around one frame per second, we developed RVFS, which uses conventional laser scanning systems (MPLSM or confocal) to perform full-field analysis of flow. Instead of requiring high frame rates, the method takes advantage of the relatively low speed of the laser field scans, which results in distortion of RBC images. RVFS is based on an analysis of the length of time a given cell spends in the scan line (that is, RBC's residence time and traveled distance) extracted from the distortion of the images of RBCs as they move during scanning. Whereas ALS and RTLS use stationary lines, RVFS uses a moving line scan. Because the line takes a finite amount of time to scan across the field, the resulting *x*–*y* image contains signals from cells that are distorted, and the distortion depends on the velocity of the cells relative to the moving scan line. RVFS analysis is then based on the relationship between RBC distortion and laser scanning velocity. The residence time is highest when the scan velocity approximates that of the moving RBCs. To fully deconvolve the velocities and generate reliable data for all vessels in the field, we needed to scan in multiple directions and speeds, and collect accurate morphological information on the vessel network (for calculating relative scan angles). Blood velocity can be resolved by comparing the residence times and the scanning velocities for scans in the same direction as the flow and fitting the data to the appropriate function (**Fig. 1b** and **Supplementary Fig. 3**; equation derived from the Doppler effect). Furthermore, we could calculate flux in a given vessel from the number of RBCs and the scanning velocities.

The RVFS imaging protocol depends on the size of the region or volume of interest. As the sampling rate of RVFS per vessel is lower than that of ALS or RTLS, physiological fluctuations in blood flow induced by heart rate or vasomotion can distort the relationship between residence time and scanning speed, potentially generating multiple peaks. At maximum residence time, as scan velocity approximates that of the moving RBCs, 'velocity-matched' RBC streaks are generated. If the resulting stretched signals are substantially longer than the size of an RBC (>4 × 7 μm), they can be used directly to analyze traveled distance and calculate velocity (**Fig. 1b** and **Supplementary Fig. 3**). Measurement of flow based on velocity-matched RBCs allows velocity to be averaged over the imaging time and minimizes the effect of temporal fluctuations. For vessels in which no velocity-matched RBCs are generated and residence time versus scanning speeds do not follow the Doppler equation, it is necessary to increase the range by scanning either faster or slower through the field.

Analysis of cross-sectional flow profiles in tumor vessels

RVFS and RTLS yield similar results when applied to the same vessel segments (**Fig. 1d** and **Supplementary Fig. 2c**). Differences in velocities measured by RVFS and RTLS appear more frequently in small vessels with relatively low RBC flux, where RVFS is less accurate (**Fig. 1d**). By using RTLS to scan through segments of vasculature undergoing intussusceptive angiogenesis[11], we recorded the first shear rate profiles around intussusceptive tissue structures (**Fig. 2**). We calculated shear rate as the difference in velocity between adjacent voxels along a vector perpendicular to the vessel wall. We observed differences in flow and shear rates between the segments separated by the interstitial tissue structures, and the shear rates varied around the perimeter of each of the segments (**Fig. 2**); this was in contrast to data for vessels not undergoing intussusception, in which the shear rate was uniform around the perimeter (**Supplementary Fig. 4**). It is possible that these shear rate gradients help to guide the insertion and growth of intussusceptive tissue structures.

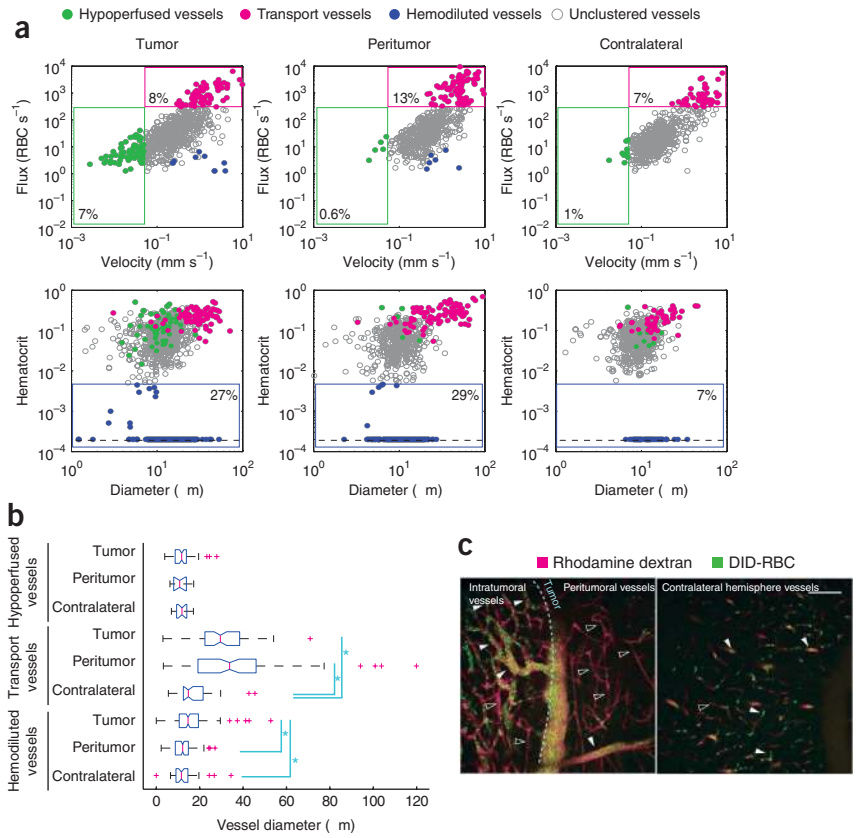

Figure 3 | Multiparametric phenotypic vessel clustering to compare vessels in tumor, peritumor and contralateral brain regions in a glioma model. (**a**) Analyses of vessels in glioma-bearing mice ($n = 6$). Scatter plots of velocity against flux and diameter against hematocrit show the gating applied to analyze the indicated vessel subtypes. (**b**) Box plots for vessel diameter from clustered vessels (*$P < 0.05$). (**c**) MPLSM micrographs of glioma vasculature (intravital images). TAMRA-BSA was used for the angiographic contrast and fluorescent RBCs (green) were injected 1 d before imaging. Glioma cells expressed GFP, which allowed accurate localization of the tumor and determination of the tumor edge (dashed line). Tumor vessels were heterogeneous with high- (closed arrowheads) and low- (open arrowheads) hematocrit vessels. Peritumor vessels were morphologically normal and had low (open arrowheads) hematocrit when compared to vessels in contralateral brain. Scale bar, 100 μm.

Multiparametric phenotypic vessel clustering

Current techniques for analyzing tumor blood vessels rely mainly on vessel structure or morphology to discriminate between vessel subtypes. To test the ability of our methodology to distinguish and analyze vessel populations, we used RTLS to measure velocities, fluxes and hematocrits of 2,351 vessels from six glioma-bearing mice (**Fig. 3**). Using GFP-expressing glioma cells, we recorded the location of each vessel relative to the tumor mass and classified each as tumor or peritumor; we also analyzed contralateral brain hemisphere vessels (**Supplementary Fig. 5a**). Considering only the average values, peritumor vessels had higher velocity, flux and wall shear rate than did tumor or contralateral brain vessels (**Supplementary Fig. 5b**). Average tumor vessel perfusion parameters (velocity and flux) were not different from those found in contralateral brain vessels (**Supplementary Fig. 5b**). By clustering the vessels into specific phenotypes (hypoperfused vessels, velocity < 0.05 mm s^{-1}; transport vessels, flux > 300 RBCs s^{-1}; and hemodiluted vessels, hematocrit < 0.005) we analyzed the relationship between vessel location and function (**Fig. 3a**). For example, there was a population of vessels, characterized by low velocity and flux, high hematocrit and variable diameter, which were more prevalent in tumor tissue (**Fig. 3a**). Transport vessels, which we defined as vessels with high flux, were present in all areas but were most abundant in the peritumor area, consistent with peritumoral arteriogenesis (**Fig. 3a**). Transport vessels had significantly ($P < 0.05$) larger diameters in the tumor and the peritumor compared to the contralateral brain, suggesting that feeding and draining vessels in these regions[4] were extensively dilated (**Fig. 3a**,**b**). Hemodiluted vessels, defined by their low hematocrit, were present in all compartments but with higher fractions in tumor and peritumor areas (**Fig. 3b**). Low hematocrit vessels in the peritumor area were morphologically normal, with diameters similar to those of vessels in normal brain and with high RBC velocity. The variation in vessel hematocrit we observed in the tumor and peritumor regions is probably due to loss of plasma by leaky vessels, which increases hematocrit. The extravasated plasma, which also increases tumor interstitial fluid pressure[12], is eventually reabsorbed by other vessels, diluting their RBCs (**Fig. 3c**). Thus, RTLS and RVFS provide a framework for distinguishing and classifying vessel populations, providing more sensitive analyses of vascular physiology in and around tumors. This approach should enable focused studies of how vessel subpopulations shift during tumor growth and in response to therapies.

DISCUSSION

Each of these techniques has advantages and disadvantages. RTLS has high sensitivity and allows cross-sectional analysis of flow in vessels, but flow analysis is limited to the location of intersection between the line and the vessel. RVFS allows analysis of entire vessel networks, integrating flow analysis at multiple positions along vessels. However, it is slower owing to the need for multiple scan angles and speeds, and its accuracy can be affected by low RBC flux. A comparison of ALS, RTLS and RVFS is presented in **Table 1**.

An important feature of RTLS is its ability to resolve velocities and fluxes spatially in individual vessels. The technique generates profiles of RBC velocity and flux (and therefore hematocrit) across each sampled blood vessel cross-section (**Fig. 1a** and **Supplementary Fig. 1**). Furthermore, when combined with measurements of vessel cross-section assessed using a second fluorophore restricted to the plasma, RTLS can be used to accurately estimate wall shear rates and stresses.

Such spatially resolved measurements of wall shear rates have the potential to answer long-standing questions of how blood shear forces exerted on endothelial cells contribute to processes such as atherogenesis and angiogenesis. For example, it is well

Table 1 | Comparison of methods for measuring blood dynamics

	ALS	RTLS	RVFS
Description			
Protocol	Repeatedly scan along a line parallel to the vessel wall (**Fig. 1a**).	Repeatedly scan along a line intersecting one or multiple vessels (**Fig. 1a** and **Supplementary Fig. 1**).	Progressively scan a line over an area. Repeat at various scan speeds and angles (**Fig. 1b** and **Supplementary Fig. 3**).
Velocity analysis	Velocity is given by the angle of the signals in the *x*–*t* image.	Velocity is extracted from the residence times of individual RBCs as they pass the scan line.	Velocity is deconvolved from the stretched RBC signal, which is determined by the relative velocity between the field scan and the RBC.
Yield	Single 'lane' in the analyzed vessel; resolution determined by resolution of laser scan.	Cross-sectional velocity profile of all intersected vessels.	Full velocity field within all vessels (in the range of sensitivity).
Sensitivity	Depends on line scan rate and line length.	Depends on line scan rate.	Depends on sampling (number of scan rate and angle variations).
Application	Monitor velocity with high time resolution in a single vessel with moderate or fast flow.	Monitor velocity and shear rate with high time resolution simultaneously in multiple vessels with moderate or slow flow.	Measure average flow velocity in all the vessels of a region or volume of interest (within a predefined range of sensitivity).
Limitations			
High RBC velocity in vessels; arterioles	Line scan rates of standard systems[a] limit sensitivity. Solution: increasing line length increases sensitivity.	Line scan rates of standard systems[a] limit sensitivity. Solution: analyze residence time at a single pixel instead of a line.	Field scan speed and angle specifications have to be optimized specifically to analyze high-velocity vessels.
Low-velocity vessels	No limitations.	No limitations.	Field scan speed and angle specifications have to be optimized specifically to analyze low-velocity vessels.
Three-dimensional vessels	Analyzes flow in the scanned plane. Velocity components perpendicular to the imaged plane are not resolved.	No limitations.	Analyzes flow in the scanned plane. Velocity components perpendicular to the imaged plane are not resolved.
Yield	Limited to a specific location in the chosen vessel. Biased to operator-selected vessels.	Generally limited to a single cross-section of each intersected vessel.	Limited to those vessels that have RBC velocity similar to the specified field scan velocity (speed and direction).
Temporal resolution	Limited by laser scan frequency (typically 500–1,000 scans per second).	Limited by laser scan frequency (typically 500–1,000 scans per second).	Typical acquisition rates: for *x*–*y* area, 12 s[b]; for *x*–*y*–*z* volume, 8 min[c].
Potential error	Accuracy of RBC *d*–*t* image angle is critical.	Accuracy of RBC residence time is critical. RBC preferential orientation can contribute error to the residence time analysis.	Accuracy of measurement of the distance traveled by the RBC is critical.
Advantages			
	Higher sensitivity than RTLS for high-velocity vessels.	Measures velocity profile and shear rates.	Measures all vessels in the area of interest.
	No need to label tracer RBCs.	Analyzes flow in penetrating and diving vessels.	
		Can analyze multiple vessels simultaneously.	

[a]Olympus confocal or multiphoton laser scanning microscope. Olympus FV300 scanning unit: 256 × 256 pixels (660 × 660 μm) scanned in 0.45 s. [b]Assumes 660 × 660 μm field sampled at six angles with two speeds at each angle. [c]Assumes 660 × 660 × 100 μm field sampled at six angles with two speeds at each angle (40 *z*-dimension slices).

known that endothelial cells sense shear stress gradients and respond by activating genes related to cell migration, vasoregulation and proliferation[13]. But as there were previously no methods for measuring shear stress gradients *in vivo*, it is not known to what extent they affect the organization or migration of endothelial cells during angiogenesis. Systematic application of RTLS during the process of angiogensis might resolve these issues. Although demonstrated here for tumor vessels, the techniques can be used to analyze any vasculature accessible by confocal or multiphoton microscopy.

METHODS

Methods and any associated references are available in the online version of the paper at http://www.nature.com/naturemethods/.

Note: Supplementary information is available on the Nature Methods website.

ACKNOWLEDGMENTS

We thank T. Padera for editorial comments and S. Roberge for technical assistance. This work was supported in part by US National Institutes of Health grants R01HL064240 (L.L.M.), R01CA149285 (L.L.M.) and P01CA80124 (R.K.J.) and by a postdoctoral fellowship from the Susan G. Komen Foundation (W.S.K.).

AUTHOR CONTRIBUTIONS

W.S.K. conceived and designed the experiment, validated and implemented the technique, collected data and wrote the manuscript. S.-S.C., D.A.L. and M.A.G. implemented the technique and collected data. J.A.T. conceived and designed the experiment and validated the technique. M.M. validated the technique. D.F. conceived and designed the experiment and provided administrative support. R.K.J. provided administrative and financial support and edited the manuscript. L.L.M. conceived and designed the experiment, provided administrative and financial support and wrote the manuscript.

COMPETING FINANCIAL INTERESTS

The authors declare competing financial interests: details accompany the full-text HTML version of the paper at http://www.nature.com/naturemethods/.

Published online at http://www.nature.com/naturemethods/.
Reprints and permissions information is available online at http://npg.nature.com/reprintsandpermissions/.

1. Fukumura, D., Yuan, F., Monsky, W.L., Chen, Y. & Jain, R.K. Effect of host microenvironment on the microcirculation of human colon adenocarcinoma. *Am. J. Pathol.* **151**, 679–688 (1997).
2. Brizel, D.M. *et al.* A comparison of tumor and normal tissue microvascular hematocrits and red cell fluxes in a rat window chamber model. *Int. J. Radiat. Oncol. Biol. Phys.* **25**, 269–276 (1993).
3. Endrich, B., Reinhold, H.S., Gross, J.F. & Intaglietta, M. Tissue perfusion inhomogeneity during early tumor growth in rats. *J. Natl. Cancer Inst.* **62**, 387–395 (1979).
4. Nagy, J.A., Chang, S.H., Dvorak, A.M. & Dvorak, H.F. Why are tumour blood vessels abnormal and why is it important to know? *Br. J. Cancer* **100**, 865–869 (2009).
5. Kamoun, W.S., Schmugge, S.J., Kraftchick, J.P., Clemens, M.G. & Shin, M.C. Liver microcirculation analysis by red blood cell motion modeling in intravital microscopy images. *IEEE Trans. Biomed. Eng.* **55**, 162–170 (2008).
6. Rosenblum, W.I. & El-Sabban, F. Measurement of red cell velocity with a two-slit technique and cross-correlation: use of reflected light, and either regulated dc or unregulated ac power supplies. *Microvasc. Res.* **22**, 225–227 (1981).
7. Kleinfeld, D., Mitra, P.P., Helmchen, F. & Denk, W. Fluctuations and stimulus-induced changes in blood flow observed in individual capillaries in layers 2 through 4 of rat neocortex. *Proc. Natl. Acad. Sci. USA* **95**, 15741–15746 (1998).
8. Brown, E.B. *et al. In vivo* measurement of gene expression, angiogenesis and physiological function in tumors using multiphoton laser scanning microscopy. *Nat. Med.* **7**, 864–868 (2001).
9. Drew, P.J., Blinder, P., Cauwenberghs, G., Shih, A.Y. & Kleinfeld, D. Rapid determination of particle velocity from space-time images using the Radon transform. *J. Comput. Neurosci*. published online, doi:10.1007/s10827-009-0159-1 (21 May 2009).
10. Lindsey, E.S., Donaldson, G.W. & Woodruff, M.F. Erythrocyte survival in normal mice and in mice with autoimmune haemolytic anaemia. *Clin. Exp. Immunol.* **1**, 85–98 (1966).
11. Patan, S. *et al.* Vascular morphogenesis and remodeling in a human tumor xenograft: blood vessel formation and growth after ovariectomy and tumor implantation. *Circ. Res.* **89**, 732–739 (2001).
12. Jain, R.K., Tong, R.T. & Munn, L.L. Effect of vascular normalization by antiangiogenic therapy on interstitial hypertension, peritumor edema, and lymphatic metastasis: insights from a mathematical model. *Cancer Res.* **67**, 2729–2735 (2007).
13. Frangos, J.A., McIntire, L.V. & Eskin, S.G. Shear stress induced stimulation of mammalian cell metabolism. *Biotechnol. Bioeng.* **32**, 1053–1060 (1988).

ONLINE METHODS

Animal models and cell lines. We implanted mammary fat pad windows or cranial windows into 8–10-week-old Tie2-GFP mice and nude mice, respectively[14]. Small mammary carcinoma (MCaIV) or glioma (U87 and GL261 used for intussusceptive angiogenesis analysis) tumor fragments (0.2–0.3 mm diameter) were implanted into the mammary fat pad or the left cerebral cortex, respectively. To spatially locate the tumor within the brain, GFP was stably transfected into U87 using a retroviral construct. All cell lines were maintained in DMEM medium with 10% FBS. All experiments were approved by the Massachusetts General Hospital Subcommittee on Research Animal Care.

Red blood cell fluorescence labeling. We labeled red blood cells *ex vivo* with 1,1-dioctadecyl-3,3,3,3-tetramethylindodicarbocyanine perchlorate (Invitrogen), a far-red lipophilic fluorescent die. Blood was collected through cardiac puncture from old donor males of the same strain used in the experiment. RBCs were separated from plasma and leukocytes by centrifugation. RBCs were diluted 1:100 in PBS (10 ml) and were incubated for 20 min with 100 µl of 1 mg ml^{-1} DID (dissolved in 95% ethanol). We washed RBCs with PBS and mixed with saline at 50% hematocrit. We injected 150–200 µl of labeled RBCs through tail veins 1–5 d before imaging. We monitored fluorescent RBC fraction *in vivo* by analyzing the normal brain capillaries. Nonfluorescent RBCs are detected in small caliber capillaries (in the brain or the mammary fat pad) through their ability to exclude TAMRA-BSA. The ratio of fluorescent to total number of RBCs is calculated at every imaging time point.

Intravital multiphoton laser scanning microscopic (MPLSM). *In vivo* multiphoton laser scanning microscopic analysis of glioblastoma and mammary carcinoma vessels was performed as described[14,15]. The MPLSM consisted of a MilleniaX pumped Tsunami Ti:sapphire laser (Spectra-Physics). Two-photon excitation of the used fluorophores (TAMRA, GFP and DID) was achieved using 840-nm light. Power at the sample was estimated to be 1–5 mW. MPLSM microscope consisted of an Olympus Fluoview FV300 system customized for multiphoton imaging. We identified the tumor area by analysis of GFP constitutively expressed by U87 (**Supplementary Fig. 5**). We performed vessel angiography after intravenous injection of 0.1 ml of 10 mg ml^{-1} TAMRA-BSA (Invitrogen). We imaged two adjacent areas in the tumor and one area in the contralateral brain by acquiring 3D stacks (dimension: 630 × 630 × 250 µm; resolution: 2.4 × 2.4 × 2.5 µm per pixel). We segmented tumor volume using a semi-automated algorithm that is based on a user-specified threshold (Matlab; Mathworks). Vessels were segmented using a tracing algorithm[16].

Residence time line scan imaging. We performed RTLS imaging by scanning along a line that intersected the vessels. In our analyses of gliomas (**Fig. 1c**), 20–40 line scans were manually positioned at various depths. To generate cross-sectional flow profiles, scanning was performed along a manually positioned line scan (blue line in **Fig. 2**) at depths ranging from 0 to 50 µm with 2.5-µm step size. At each depth we scanned 3,000–4,000 lines at a resolution of 2.5 µm per pixel in the *x*–*y* plane with one line per 1.3–1.5 ms. We performed phenotypic clustering of glioma vessels by scanning along a pseudogrid that randomizes vessel selection. While collecting the line scans, a snapshot of the analyzed plane was imaged and used to determine the orientation of the intersected vessels (**Fig. 1a** and **Supplementary Fig. 1**). We segmented RBCs and extracted residence times using a computer-assisted semi-automated in-house algorithm (coded in Matlab). The velocity of each RBC was calculated using the equation presented in **Figure 1b**. We analyzed vessel profiles by determining the RBCs flowing at each lane in the cross-section of the vessel. RBC flux reflects the total number of RBCs per second. Hematocrit was measured as the fraction of RBC pixels over the total number of pixels within the lane. RBC *z* resolution was measured by imaging stationary RBCs within 0.5-mm microchannels (RBC *z*-dimension resolution, 10 µm).

Relative velocity field scanning. The imaging protocol for RVFS consists of imaging the same field at various scanning velocities. Using a conventional MPLSM system, we performed repetitive 3D imaging of the vessels at variable scanning velocities (1.53, 1.16, 0.78 and 0.39 mm s^{-1}) and at various resolutions (1.3 and 2.5 µm per pixel). As vessels have various orientations, the projected scanning velocity over the vessel axis is different for each vessel and is higher than the vertical velocity. To ensure all vessels were scanned along the RBC flow direction, imaging was performed at four rotation angles: 0°, 90°, 180° and 270°. To align the volumes and correct for microscope-related drift, a rigid registration algorithm was implemented based on 3D normalized cross-correlation. Vessel networks were traced and subdivided into single vessel segments of equal length (50 µm). In each vessel, we determined the residence times for segmented RBCs and fit them to the scanning velocity adjusted to the vessel angle. RBC tracks representing a traveled distance greater than four times the length of an RBC (28 µm) were directly identified and analyzed to extract travel distance and calculate velocity.

Shear rate calculation. We calculated vessel shear rate from the gradient of RBC velocities in adjacent lanes in the blood vessel. The lanes are defined by image pixels. For each lane, we calculated RBC velocity as the mean velocity of all the RBCs passing through. Thus, in general, each RBC is present in more than one lane, most often two lanes, and therefore contributes to the average flow, hematocrit and flux of those lanes.

For the cross-sectional analysis of flow (**Fig. 2** and **Supplementary Fig. 4**), we generated shear rate maps by calculating the average shear rate for each pixel at the resolution of 2.5 µm per pixel. Shear rate is equal to the average difference in velocity between the two adjacent pixels, divided by the distance. For the clustering experiment (**Fig. 3** and **Supplementary Fig. 5**), we calculated shear rate using two approaches. Mean shear rate is the velocity gradient in the entire vessel cross-section along the RTLS divided by distance (data not included). Wall shear rate is the velocity gradient at the vessel wall calculated as the velocity in the lane closest to the vessel wall divided by the distance (assuming that the velocity at the vessel wall is 0 mm s^{-1}).

Statistical analysis. Data are expressed as mean ± s.e.m. The principal statistical test was the Student's *t*-test (two-tailed with unequal variance). We analyzed the experiments involving multiple comparisons using multivariate analysis of variance followed by post-hoc within

and between groups hypothesis testing (SYSTAT 12, SYSTAT Inc.). We considered a *P*-value less than 0.05 to be statistically significant.

14. Jain, R.K., Munn, L.L. & Fukumura, D. Dissecting tumour pathophysiology using intravital microscopy. *Nat. Rev. Cancer* **2**, 266–276 (2002).
15. Winkler, F. *et al.* Kinetics of vascular normalization by VEGFR2 blockade governs brain tumor response to radiation: role of oxygenation, angiopoietin-1, and matrix metalloproteinases. *Cancer Cell* **6**, 553–563 (2004).
16. Tyrrell, J.A. *et al.* Robust 3-D modeling of vasculature imagery using superellipsoids. *IEEE Trans. Med. Imaging* **26**, 223–237 (2007).

doi:10.1038/nmeth.1475